Advances in Engineering Software 142 (2020) 102749

Contents lists available at ScienceDirect

Advances in Engineering Software

journal homepage: www.elsevier.com/locate/advengsoft

Research paper

Stochastic design of double-skin façades as seismic vibration absorbers

Giovanni Pipitone, Giorgio Barone, Alessandro Palmeri*

Loughborough University, School of Architecture, Building and Civil Engineering, Sir Frank Gibb Building, Loughborough, Leics LE11 3TU, UK

ARTICLE INFO

Keywords:
Double skin façade
Earthquake engineering
Passive control
Primary-secondary dynamic interaction
Random vibration theory
Structural optimisation

ABSTRACT

Double-skin façades (DSFs), usually designed for aesthetic reasons or energy saving purposes, have been recently proposed as an alternative mean of passive control, able to reduce the effects of dynamic actions on building structures. This paper presents a novel approach to optimise their design as distributed vibration absorbers (VAs). Four key design parameters have been chosen to represent the façade, namely its flexural stiffness and viscous damping ratio, along with the stiffness of the elements connecting the façade to the primary structure. The optimisation is achieved by minimising the variance of the building's dynamic response, conveniently computed in a stochastic framework. Solutions are obtained using genetic algorithms (GAs), including nonlinear constraints limiting the relative displacements between primary and secondary structures. Computational efficiency of the optimisation procedure is largely improved, compared to previous works, by characterising the seismic action as a stationary random process, fully defined by some closed-form analytical expressions for the power spectral density (PSD) function consistent with target response spectra. Four configurations of double-skin façades have been analysed, including single and multi-panel layouts, spanning one to six storeys, and their efficiency has been quantified. Results are compared with those obtained directly in the time domain by numerical integration of the equations of seismic motion for a suite of recorded accelerograms, showing a good level of consistency.

1. Introduction

Seismic events are random in nature, and several methods have been proposed in the technical literature to account for their inherent randomness when designing earthquake-resistant structures [8]. In particular, the seismic action can be properly modelled as a coloured random process, which in turn enables the evaluation of the seismic response using the random vibration theory [28]. If the external excitation constitutes the only source of randomness, then the conventional stochastic structural optimisation (CSSO) method can be used to determine optimal values of the deterministic design parameters. One of the pioneering applications of this technique can be found in the work by Nigam [22], in which the optimal design parameters of an aeronautic structural component have been found by modelling the aerodynamic load as random processes. In the vibration control of civil engineering structures, several studies have used the CSSO theory to design damping devices, including Refs. [14,16,21]. In Ref. [9], the optimal damping coefficients of seismic control devices installed into a shear-type frame have been obtained as solution of an optimisation problem where the standard deviation of the displacement of the first storey has been minimised. In several studies, it has been shown that metaheuristic algorithms can be powerful tools to approach this kind of optimisation problems. For example, Marano et al. [17] developed a robust optimal design criterion for tuned mass dampers (TMDs), where the ground acceleration is conveniently modelled as a stationary white noise and the structural performance has been optimised using genetic algorithms (GAs). Similarly, in Ref. [19], the design of multiple TMDs (MTMDs) has been achieved using GAs, considering the structure excited by a wind pressure field. The latter is modelled as a white noise, and the results of this study confirms the capability of MTMDs to control multiple modes of vibration, thus reducing the vibrational energy over a wider range of frequencies.

In recent years, the application of double-skin façades (DSFs) as mass vertical distributed dampers has been suggested. A DSF is a building envelope installed over the main structure aiming at improving the energy performance of the building and the whole aesthetics. Usually realised in steel and glass, the DSF provides a better ventilation (natural or mechanical), increases the thermal insulation and also reduces the penetration of external noise [6,12,13]. Previous research carried out on the DSFs as vibration absorbers (VAs) has been performed assuming the external excitation as deterministic. Fu et al. [11] investigated the application of DSFs to reduce the vibration

* Corresponding author.
E-mail addresses: A.Palmeri@Lboro.ac.uk, Dynamics.Structures@gmail.com (A. Palmeri).

https://doi.org/10.1016/j.advengsoft.2019.102749
Received 14 February 2019; Received in revised form 23 October 2019; Accepted 3 November 2019
Available online 19 February 2020

induced by a set of earthquake records, and different configurations have been compared, finding that DSF substructures spanning multiple storeys tend to perform better than having DSF panels acting as independent TMDs at each storey. Moon [1,20] presented a control system based on a DSF arranged as a set of vertically distributed mass dampers under wind load. Bedon et al. [4,5] modelled the DSF as a series of vertical distributed TMDs. In particular, in Ref [5] the authors proposed a model in which the edges of each DSF panel are connected to the main structure by elements formed by a spring and a viscous damper. The whole system is excited by earthquake and blast loads. The analyses are carried out comparing the model proposed with a conventional building-DSF system (i.e. connected using rigid elements). The results show the effectiveness of the DSF as MTMD to absorb the vibrational energy with respect to the classical façade design. Moreover, the authors advise to have at least one connection between DSF and building at each storey level aiming to avoid large displacements of the façade. Similar outcomes are also suggested by Parsaeimaram et al. [24], where the authors investigated the effects of removing or adding the connection beams between a base isolated building and the DSF.

A lumped-mass model of DSF, connected to the primary load-bearing structure by elastic links, has been proposed in previous works by Palmeri et al. [23] and Pipitone et al. [25]. In these studies, the performance of various configurations of DSFs as seismic VAs has been optimised using metaheuristic algorithms. Various numbers of independent DSF substructures have been considered, spanning from one to six storeys. The optimisation was based on the deterministic structural response to a pre-selected set of earthquake records. The authors showed the feasibility of designing an effective DSF-type of VA, provided a large enough set of accelerograms is used in the optimisation phase. The latter however entails the drawback of requiring a large number of time-history dynamic analyses and, consequently, a high computational effort.

In this paper, a novel approach for the optimisation of DSFs as VAs for earthquake engineering applications is proposed, in which the seismic excitation is conveniently modelled as a stationary zero-mean Gaussian process, fully characterised by its power spectral density (PSD) function. The latter is defined through the analytical model proposed in Refs. [2,3], which is consistent with response spectra proposed by Eurocode 8 [7] and other international building codes. In contrast to previous research, using a stochastic model for the ground acceleration allows applying random vibration analysis tools directly in the frequency domain, which in turn results in significant savings in terms of computational time. The design of DSFs has been approached as an optimisation problem in which the design variables are: *i*) the flexural stiffness of the outer-skin panels, spanning from one to six storeys; *ii*) the stiffness of the spring elements connecting the DSF to the main building structure; and *iii*) the viscous damping ratio of the DSF. The optimal values of these design parameters have been determined by minimising the variance of the displacements of the first storey in the building structure, taken as an engineering demand parameter (EDP) representative of the performance of the building in relation to its structural integrity.

Differently from previous investigations, this study introduces a non-linear constraint on the maximum relative displacement between the DSF and the building structure, in order to ensure the integrity of all subsystems. Results are reported varying the reference peak ground acceleration (PGA). Various configurations of links between façade and building are presented, considering the panels either connected on their edges, or in their internal points, or both. Outcomes of the proposed stochastic approach are compared with the design parameters returned by deterministic analysis based on earthquake records to show results consistency.

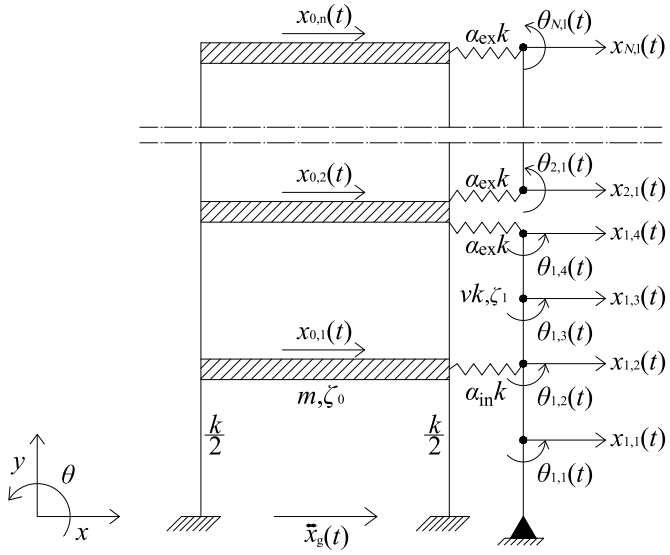

Fig. 1. Structural model.

2. Governing equations

Let's consider an *n*-storey shear-type frame, representing a multi-storey building structure, connected by elastic springs to a DSF consisting of *N* independent vertical panels of equal height, spanning one or more storeys. The building is assumed to be regular in plan, so that the analyses can be carried out on a 2D model, and in elevation, meaning that its storeys have equal mass *m*, lateral stiffness *k* and inter-storey height *h*; the viscous damping ratio in all the building's modes of vibration (when disconnected from the DSF) is ζ_0. The dynamically significant DOFs (degrees of freedom) of the building structure can then be collected in the $(n \times 1)$ vector $\mathbf{x}_0(t) = \{x_{0,1}, x_{0,2}, \cdots, x_{0,n}\}^\top$, where the subscript 0 and superscript $\top$ stand for the main structure and the transpose operator, respectively.

Considering the same model defined in Refs. [23,25], a system of ℓ_i lumped masses, equally spaced by $h/2$, is considered for the *i*th DSF panel, with $\ell_1 = 2n/N$ and $\ell_2 = \cdots = \ell_N = \ell_1 + 1$ for $N \geq 2$. Two DOFs are considered for each mass (see Fig. 1), namely the horizontal displacement $x_{i,j}(t)$ and the rotation $\theta_{i,j}(t)$, in which $i = 1, 2, \cdots, N$ is the number of the DSF panel and $j = 1, 2, \cdots \ell_i$ is the number of the masses along the height of the *i*th panel. The DOFs of the full panel can then be collected in the $(2\,\ell_i \times 1)$ vector $\widetilde{\mathbf{x}}_i(t) = \{x_{i,1}, \cdots, x_{i,\ell_i}, \theta_{i,1}(t), \cdots, \theta_{i,\ell_i}(t)\}^\top = \{\mathbf{x}_i^\top(t) \;\; \boldsymbol{\theta}_i^\top(t)\}^\top$, where $\mathbf{x}_i(t)$ and $\boldsymbol{\theta}_i(t)$ list the translational and rotational DOFs of the *i*th DSF subsystem, respectively.

The equations of motion for the coupled building-DSF dynamic system can be written in compact matrix form as:

$$\mathbf{M}\cdot\ddot{\mathbf{x}}(t) + \mathbf{C}\cdot\dot{\mathbf{x}}(t) + \mathbf{K}\cdot\mathbf{x}(t) = -\mathbf{M}\cdot\boldsymbol{\tau}\,\ddot{x}_g(t)\,, \tag{1}$$

where, after a static condensation of the rotational DOFs in the DSF panels, the super-vector $\mathbf{x}(t) = \{\mathbf{x}_0^\top(t) \;\; \mathbf{x}_1^\top(t) \;\; \cdots \;\; \mathbf{x}_N^\top(t)\}^\top$ collects the dynamically significant DOFs of all the subsystems; the central dot $\cdot$ indicates the matrix product; $\boldsymbol{\tau} = \mathbf{1}_{3n+N-1}$ is the corresponding incidence vector of the seismic action, $\mathbf{1}_s$ being a unit vector of size *s*; $\ddot{x}_g(t)$ is the ground acceleration; $\mathbf{M}$ and $\mathbf{K}$ are block matrices, which can be conveniently written as follows:

$$\mathbf{M} = \begin{bmatrix} \mathbf{M}_0 & \mathbf{O}_{n\times\ell_1} & \cdots & \mathbf{O}_{n\times\ell_N} \\ \mathbf{O}_{\ell_1\times n} & \mathbf{M}_1 & \cdots & \mathbf{O}_{\ell_1\times\ell_N} \\ \vdots & \vdots & \ddots & \vdots \\ \mathbf{O}_{\ell_N\times n} & \mathbf{O}_{\ell_N\times\ell_1} & \cdots & \mathbf{M}_N \end{bmatrix}; \tag{2a}$$

$$\mathbf{K} = \begin{bmatrix} \mathbf{K}_0 & \mathbf{K}_{01} & \cdots & \mathbf{K}_{0N} \\ \mathbf{K}_{01}^\top & \mathbf{K}_1 & \cdots & \mathbf{O}_{\ell_1 \times \ell_N} \\ \vdots & \vdots & \ddots & \vdots \\ \mathbf{K}_{0N}^\top & \mathbf{O}_{\ell_N \times \ell_1} & \cdots & \mathbf{K}_N \end{bmatrix}, \tag{2b}$$

where $\mathbf{M}_0$ and $\mathbf{K}_0$ are the $(n \times n)$ mass and stiffness matrices of the primary structure; $\mathbf{M}_i$ and $\mathbf{K}_i$ are the $(\ell_i \times \ell_i)$ mass and stiffness matrices of the DSF panels (as obtained by statically condensing their rotational DOFs), and each out-of-diagonal $(n \times \ell_i)$ block $\mathbf{K}_{0i}$ contains the stiffness of the elastic links coupling primary structure and ith DSF panel. The panels' flexural stiffness (assumed to be the same for all the N DSF panels) and the stiffness of the links are expressed in the following as proportional to the building's storey stiffness k through the non-dimensional coefficients ν, α_{ex} and α_{in} (see Fig. 1). The damping matrix $\mathbf{C}$ for the coupled system is determined under the assumption that each subsystem is classically damped, with all the DSF panels having the same damping ratio ζ_1 (more details can be found, for instance, in Refs. [15] and [25]).

If the ground acceleration $\ddot{x}_g(t)$ is modelled as a stationary zero-mean Gaussian process of given real-valued one-sided PSD function, $G_{\ddot{x}_g}(\omega)$, the seismic response of the linear coupled system can be determined in terms of the corresponding PSD matrix of its DOFs, given by:

$$\mathbf{G}_{\mathbf{x}}(\omega) = \mathbf{H}(\omega) \cdot \mathbf{L} \cdot \mathbf{L}^\top \cdot \mathbf{H}(\omega)^{*\top} G_{\ddot{x}_g}(\omega), \tag{3}$$

where the $((3n + N - 1) \times (3n + N - 1))$ system's transfer matrix $\mathbf{H}(\omega)$ and the $((3n + N - 1) \times 1)$ array $\mathbf{L}$ are defined as:

$$\mathbf{H}(\omega) = [\mathbf{K} - \omega^2 \mathbf{M} + \imath\omega \mathbf{C}]^{-1}; \tag{4a}$$

$$\mathbf{L} = -\mathbf{M} \cdot \boldsymbol{\tau}; \tag{4b}$$

$\imath = \sqrt{-1}$ is the imaginary unit, and the superscript * stands for complex conjugate.

In the following, the PSD function $G_{\ddot{x}_g}(\omega)$ is assumed to be consistent with an assigned code-compliant elastic design (ED) spectrum, described by a four-branch piecewise equation (such as in Eurocode 8 [7]):

$$S_{\text{ED}}(T) = \begin{cases} S_0 \left[1 + (a_g - 1)\dfrac{T}{T_B}\right], & 0 \le T < T_B; \\ a_g S_0, & T_B \le T \le T_C; \\ a_g S_0 \dfrac{T_C}{T}, & T_C < T \le T_D; \\ a_g S_0 \dfrac{T_C T_D}{T^2}, & T > T_D. \end{cases} \tag{5}$$

In Eq. (5), a_g is the peak ground acceleration (PGA) on a rigid soil, S_0 is the soil amplification factor, while T_B, T_C and T_D define the intervals of periods for the four branches of the ED spectrum.

Adopting the analytical expressions proposed in Ref. [2,3], the PSD function of the ground acceleration can be expressed as:

$$G_{\ddot{x}_g}(\omega) = \begin{cases} G_0 \left(\dfrac{\omega_D}{\omega_C}\right)^{e_2} \left(\dfrac{\omega}{\omega_D}\right)^{e_1}, & 0 \le \omega \le \omega_D; \\ G_0 \left(\dfrac{\omega}{\omega_C}\right)^{e_2}, & \omega_D < \omega \le \omega_C; \\ G_0 \left(\dfrac{\omega}{\omega_C}\right)^{e_3}, & \omega_C < \omega \le \omega_B; \\ G_0 \left(\dfrac{\omega_B}{\omega_C}\right)^{e_3} \left(\dfrac{\omega}{\omega_B}\right)^{e_4}, & \omega > \omega_B, \end{cases} \tag{6}$$

where $\omega_B = 2\pi/T_B$, $\omega_C = 2\pi/T_C$ and $\omega_D = 2\pi/T_D$, and the parameters G_0, e_1, e_2, e_3 and e_4 are determined in closed form as functions of the parameters of the ED spectrum using the formulae described in [2,3] and reported in Appendix A.

3. Optimisation of the DSF structural parameters

Four different DSF layouts have been analysed, with individual DSF panels spanning from one to six storeys of the primary structure, optimising in each case the following design parameters:

1. the viscous damping ratio of the DSF: all DSF subsystems have been assumed as classically damped, with the same inherent viscous damping ratio ζ_1, which has then been chosen as a design variable;
2. the flexural stiffness of the DSF panels: in this case, the non-dimensional parameter ν has been used as design variable, assigning to all the DSF panels the same flexural stiffness $EI = \nu\, k\, h^3$, proportional to the lateral stiffness of the primary building structure;
3. the stiffness of the external links: the lumped masses at the top and bottom ends of each panel are connected to the primary structure with elastic springs, whose stiffness is assumed to be proportional to the lateral storey stiffness k of the main building through the non-dimensional coefficient α_{ex}, that is $k_{\text{ex}} = \alpha_{\text{ex}}\, k$;
4. the stiffness of the internal links: analogously, the inner nodes of the DSF panels are connected to the storey of the main structure at the same height with springs having, also in this case, stiffness proportional to the lateral storey stiffness k, $k_{\text{in}} = \alpha_{\text{in}}\, k$, and in general $k_{\text{in}} \neq k_{\text{ex}}$.

Optimal values have been defined as those minimising the variance of the displacements of the first storey of the controlled primary structure, normalised with respect to the variance of the displacements of the same storey in the uncontrolled configuration (i.e. without the façade). Hence, the following objective function has been defined:

$$J_N = \frac{\sigma^2(x_{0,1}^{(c)})}{\sigma^2(x_{0,1}^{(u)})}, \tag{7}$$

and where the superscripts (u) and (c) mean uncontrolled and controlled configuration, respectively; accordingly, the less J_N, the better the performance of the DSF.

The solution of the optimisation problem has been pursued using the generic algorithms (GAs) available in the MATLAB's optimisation toolbox [18], introducing a nonlinear constraint in order to limit the relative movement of the façade with respect to the primary structure. To do this, the deformations in all the building-to-DSF links have been considered, which can be expressed as:

$$\delta_r(t) = x_{i,j}(t) - x_{0,s}(t) = \mathbf{a}_r^\top \cdot \mathbf{x}(t), \tag{8}$$

where the rth link, with $r = s + i - 1$, connects the sth storey of the main building with the ith DSF panel (accordingly, $s = 1, 2, \cdots, n$; $i = 1, 2, \cdots, N$; $r = 1, 2, \cdots, n + N - 1$). It is worth noting that the associated incidence vector $\mathbf{a}_r$ contains $3n + N - 1$ elements (i.e. as many elements as the number of degrees of freedom of the coupled system with statically-condensed DSF panels); these are all zeros apart from 2 elements, namely: the sth element equal to -1 (that is, the element corresponding to the sth storey of the main structure) and the element kth equal to $+1$, corresponding to the jth lumped mass in the ith panel connected to the link. It can be shown that: $k = n + j + (i - 1)\ell_1 + (i - 2)$; the index j spans all the even numbers $\le \ell_1$ for $i = 1$ and all the odd numbers $\le \ell_i$ for $i \ge 2$.

Since the seismic input has been modelled as a zero-mean Gaussian process, and the coupled building-DSF dynamic system is linear, the generic relative displacement $\delta_r(t)$ is also a zero-mean Gaussian process. The rth demand parameter $\Delta_{r,p}$ can now be introduced as the lower pth percentile of the absolute maximum of $\delta_r(t)$ during the duration of the strong-motion phase T_g of the seismic event (assumed herein as the stationary duration of the seismic response), that is:

$$\text{Prob}[\max\{|\delta_r(t)|,\ 0 \le t \le T_g\} \le \Delta_{r,p}] = p. \tag{9}$$

Within a stochastic setting, $\Delta_{r,p}$ can be calculated as:

$$\Delta_{r,p} = \eta_{r,p}\,\sigma(\delta_r)\,, \tag{10}$$

where $\sigma(\delta_r)$ is the standard deviation of the random process $\delta_r(t)$ and $\eta_{r,p}$ is the associated peak factor, for which Vanmarcke's formulation can be adopted [27]:

$$\eta_{r,p} = \sqrt{2\ln\{2\,Z_{r,p}[1-\exp(-q_r^{1.2}\sqrt{\pi\ln(2\,Z_{r,p})})]\}}\,, \tag{11}$$

in which:

$$Z_{r,p} = \sqrt{\frac{\lambda_2(\delta_r)}{\lambda_0(\delta_r)}}\,\frac{T_g}{2\pi}\,[-\ln(p)]^{-1}\,; \tag{12a}$$

$$q_r = \sqrt{1-\frac{\lambda_1^2(\delta_r)}{\lambda_0(\delta_r)\,\lambda_2(\delta_r)}}\,, \tag{12b}$$

in which $\lambda_j(\delta_r)$ ($j = 0, 1, 2$) is the jth spectral moment of the process $\delta_r(t)$, defined as:

$$\lambda_j(\delta_r) = \int_0^{+\infty} \omega^j\, G_{\delta_r}(\omega)\,\mathrm{d}\omega\,, \tag{13}$$

where the one-sided PSD function of $\delta_r(t)$ can be expressed as:

$$G_{\delta_r}(\omega) = \mathbf{a}_r^{\top}\cdot\mathbf{G}_{\mathbf{x}}(\omega)\cdot\mathbf{a}_r\,. \tag{14}$$

In order to investigate how the constraint on the link deformations $\Delta_{r,p}$ affects the optimal design of the DSF, the PGA has been chosen as IM (intensity measure) of the seismic input, and the nonlinear optimisation problem summarised in Eq. (15) has been solved for increasing values of the IM:

$$\text{Given:}\quad m,\ k,\ \zeta_0,\ G_{\ddot{x}_g}(\omega),\ \text{geometry}\,; \tag{15a}$$

$$\text{Find:}\quad \zeta_1,\ \nu,\ \alpha_{ex},\ \alpha_{in}; \tag{15b}$$

$$\text{To minimise:}\quad J_N; \tag{15c}$$

$$\text{Such that:}\quad \begin{cases} \zeta_{min} \le \zeta_1 \le \zeta_{max}; \\ \nu_{min} \le \nu \le \nu_{max}; \\ \alpha_{min} \le \alpha_{in} \le \alpha_{max}; \\ \alpha_{min} \le \alpha_{ex} \le \alpha_{max}; \end{cases} \tag{15d}$$

$$\text{And:}\quad \Delta_{r,p} \le b\,,\quad r = 1, 2, \cdots, n+N-1\,, \tag{15e}$$

where the PSD function of the seismic excitation is proportional to the square of the PGA (that is, $G_{\ddot{x}_g}(\omega) \propto a_g^2$); ζ_{min}, ν_{min}, α_{min}, and ζ_{max}, ν_{max}, α_{max}, represent, respectively, the lower and upper bounds of the design parameters, defining the search space of the optimisation problem; b is the barrier value that defines the nonlinear constraint on the relative displacement between DSF panels and the main building structure.

4. Case study

The numerical analyses in the following sections have been performed considering as case study the 6-storey shear-type frame introduced in Ref. [23]. The primary structure's first fundamental period of vibration is $T_{0,1} = 0.582$ s and its damping ratio is $\zeta_0 = 0.02$. The total mass of the DSF is taken as 10% of the mass of the primary structure, and four different layouts of DSF have been studied, as shown in Fig. 2.

The seismic hazard has been defined using the same set of recorded accelerograms presented in Ref. [25]. This enables a direct comparison between some of the results presented in the two papers. More precisely:

1. The linear elastic response spectra, $S_{el,e}(T)$, for the 20 earthquake records $\ddot{x}_{g,e}(t)$ listed in Table 1 have been preliminary computed, assuming 5% of linear viscous damping ratio, with $i = 1, 2, \cdots, 20$;
2. All earthquake records have been scaled to return the same spectral acceleration at the first modal period of the uncontrolled primary case study structure, that is $\hat{S}_{el,1}(T_{0,1}) = \hat{S}_{el,2}(T_{0,1}) = \cdots = \hat{S}_{el,20}(T_{0,1})$ (Fig. 3, gray lines); this has been done because the spectral ordinate at the fundamental period of vibration is highly correlated with the amplitude of the dynamic response for a given seismic event (e.g. Ref. [26]);
3. The corresponding average spectrum has been determined (Fig. 3, red dashed line):

$$\overline{S}_{el}(T) = \frac{1}{20}\sum_{i=1}^{20}\hat{S}_{el,e}(T)\,; \tag{16}$$

4. The least square method has been used to evaluate the parameters of the target 4-branch ED spectrum of Eq. (5) that best fits $\overline{S}_{el}(T)$ (Fig. 3, black solid line);
5. Finally, the closed-form expressions of Eq. (A.1,A.2) have been used to calculate the parameters of the PSD function of Eq. (6), assuming a strong-motion phase of $T_g = 20$ s.

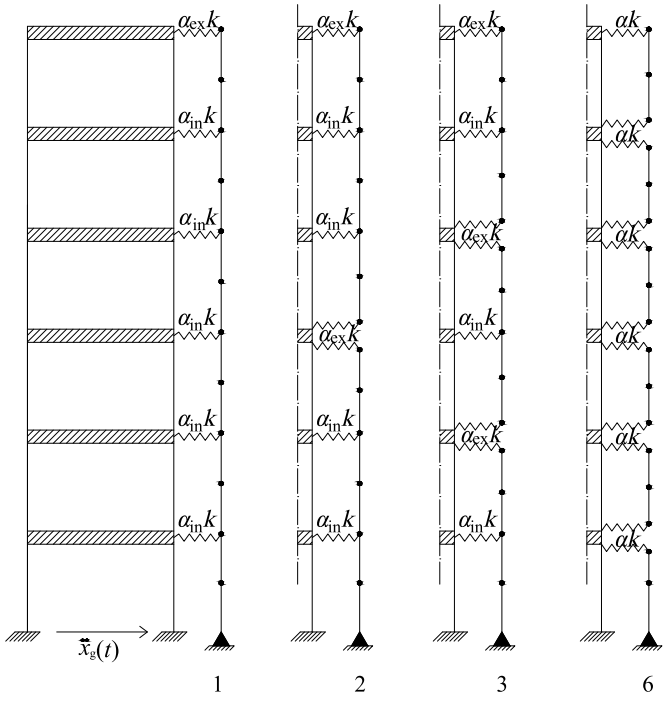

Fig. 2. 4 DSF layouts, namely 1-panel, 2-panels, 3-panels and 6-panels.

Table 1
Set of earthquake records used for the evaluation of the RS.

No.	Epicentre	Date	Peak acc. [g]	Duration [s]
1	Parkfield, California	27/06/1966	0.434	44.04
2	Pacomia Dam, California	09/02/1971	1.075	41.74
3	Helena, Montana	31/10/1935	0.147	50.96
4	Wrightwood, California	12/09/1970	0.198	16.72
5	Lake Hughes, California	09/02/1971	0.146	37.02
6	Iverson, Canada	23/12/1985	1.102	20.34
7	Yoneyama Bridge, Japan	26/02/1971	0.151	17.06
8	El Centro, California	18/05/1940	0.348	53.74
9	T. Lincon School Tunnel, California	21/07/1952	0.179	54.40
10	Monte Negro, Yugoslavia	19/04/1979	0.171	40.40
11	La Villita, Guerrero Array, Mexico	19/09/1985	0.123	64.02
12	El Centro, California	30/12/1934	0.160	44.04
13	Sturno, Italy	11/11/1980	0.358	39.34
14	Duzce, Turkey	12/11/1999	0.535	25.89
15	Takatori, Japan	16/01/1995	0.611	40.96
16	Tabas, Iran	16/09/1978	0.836	32.84
17	Erizikan, Turkey	13/03/1992	0.515	21.31
18	Kalamata, Greece	13/09/1986	0.248	12.19
19	Loma Prieta, California	18/10/1989	0.966	25.00
20	Tolomezzo, Italy	06/05/1980	0.351	36.35

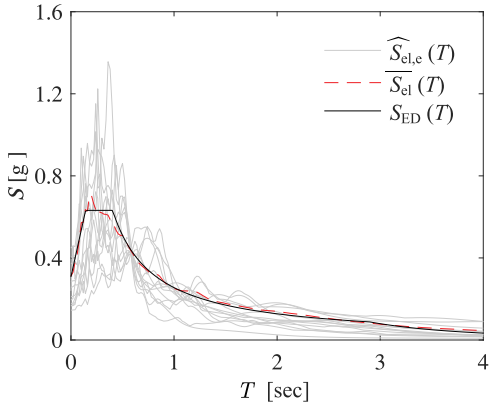

Fig. 3. RS of the 20 earthquake records ($\hat{S}_{el,e}(T)$ gray lines), average one ($\overline{S}_{el}(T)$ red dashed line) and design one ($S_{ED}(T)$ black solid line).

Table 2
Numerical parameters of design RS and coherent PSD.

RS Parameter	Value	PSD Parameter	Value
a_g	0.4 g	G_0	$1.12 \times 10^{-3} g^2/(rad/sec)$
S_0	2.0523	e_1	2.4885
T_B	0.142 *sec*	e_2	0.7519
T_C	0.404 *sec*	e_3	-1.3255
T_D	2.991 *sec*	e_4	-2.5439

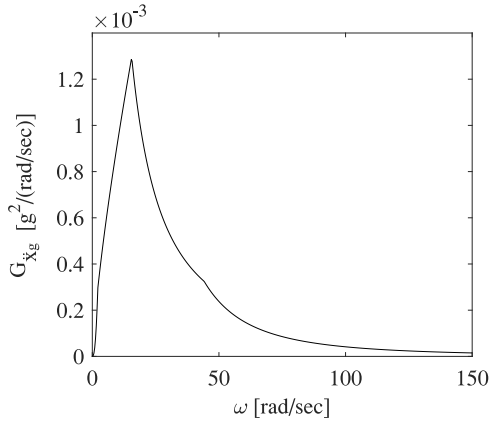

Fig. 4. PSD function coherent with the RS.

Table 2 offers the parameters of both the target ED spectrum, $S_{ED}(T)$, and the corresponding one-sided PSD function $G_{\ddot{x}_g}(\omega)$. The PSD function so determined is depicted in Fig. 4, showing a concentration of energy around $\omega_C = 2\pi/T_C = 15.54$ rad/s.

In all the numerical analyses, the optimal design parameters have been determined using the elitist GA implemented in Matlab [10]. Consistently with the deterministic optimisations presented in Ref. [25], the search space for the four design parameters has been restricted to :

$$\begin{cases} 10^{-4} \le \zeta_1 \le 0.2\,; \\ 10^{-4} \le \nu \le 0.25\,; \\ 10^{-6} \le \alpha_{ex} \le 0.05 \\ 10^{-6} \le \alpha_{in} \le 0.05\,; \end{cases} \tag{17}$$

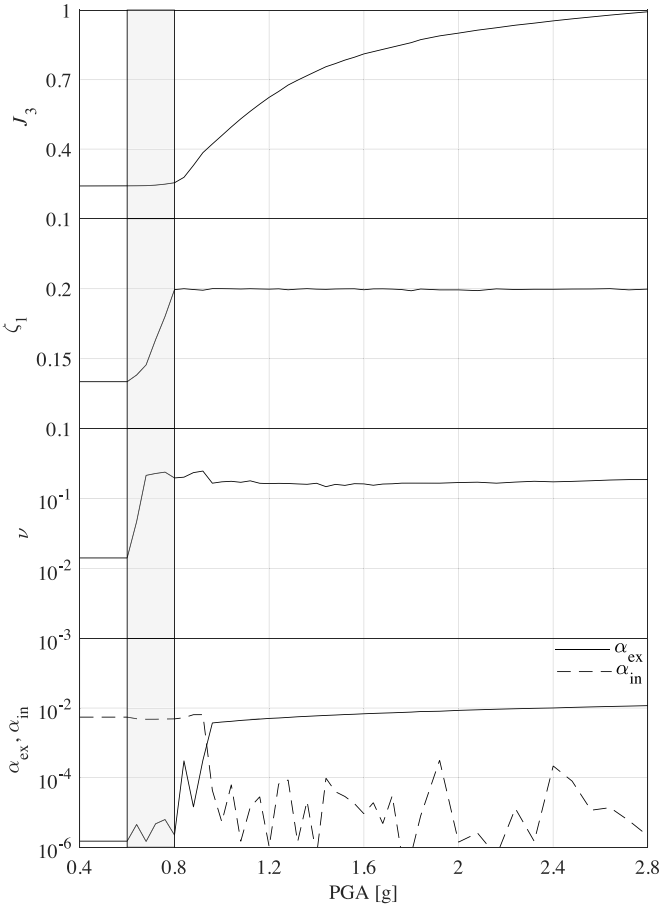

Fig. 5. Objective function and optimal design parameters for 3-panels layout.

For the nonlinear constraint, the 95% lower fractile (i.e. $p = 0.95$) of the maximum relative displacements between DSF and primary structure has been monitored, setting its limit value to $b \le 5$ cm. For each DSF layout, optimal design variables have been determined varying the PGA a_g of the ED spectrum from 0.4 to 2.8 g, with increments of 0.04 g. It has been observed that values of a_g higher than 2.8 g do not return optimal solutions compatible with the applied constraints on $\Delta_{r,0.95}$.

Fig. 5 shows the objective function J_3, optimal damping ratio ζ_1, optimal flexural coefficient ν and optimal link stiffness α_{ex} and α_{in} computed for the DSF layout with $N = 3$ panels (each one spanning 2 storeys). In this figure, three main regions can be identified for varying value of the PGA, namely:

- PGA < 0.6 g: all the optimal design parameters and the objective function show constant values. Since all the relative displacements between the DSF panels and the primary structure, $\Delta_{r,0.95}$, are always below the imposed threshold of $b = 5$ cm, the nonlinear constraint plays no role in the optimisation (that is, removing the constraint would not alter the optimal solution); the efficiency of the DSF is maximum in this range, with a reduction of the seismic response of about 76%;
- 0.6 g < PGA < 0.8 g: in order to satisfy the nonlinear constraint, panels' stiffness and damping tend to increase with the value of the PGA, while no significant variations are observed in the stiffness of the links (apart from the noise caused by the heuristic nature of the

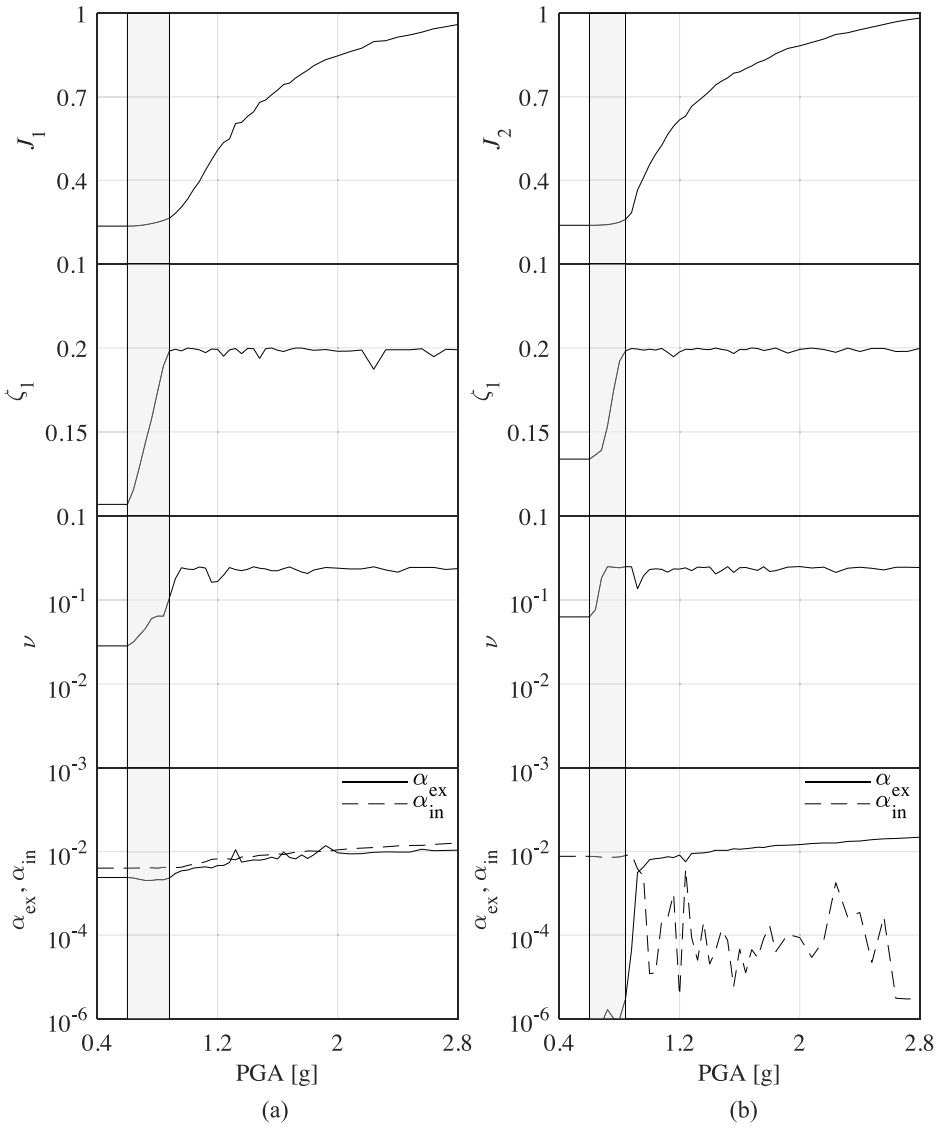

Fig. 6. Objective functions and optimal design parameters for the layouts with 1 and 2 panels.

optimisation algorithm); only a slight loss of efficiency of the control system is observed in this range, with a reduction of the seismic response from 76% to 75%.

- 0.8 g < PGA < 2.8g: once both the panels' viscous damping ratio ζ_1 and flexural stiffness coefficient ν have reached their maximum values (based on the constraints imposed on the search space) at about $a_g = 0.8\,g$, they tend to keep approximately constant values when the PGA further increases, while the stiffness of the links changes to satisfy the nonlinear constraint; this results in stiffer connection between panels and the structure and a monotonic loss of their efficiency.

It is worth noting here that the plots of ν, α_{ex} and α_{in} are semi-logarithmic, and indeed, in general, α_{ex} and α_{in} differ of several orders of magnitude. Interestingly, the external links tend to be stiffer than the internal ones for low values of the PGA, while the opposite happens for $a_g > 0.9\,g$. This swap is an effect of the nonlinear constraint.

Similar trends can be observed in Fig. 6 for the layouts with $N = 1$ and $N = 2$ panels (spanning, respectively, 6 and 3 storeys), although the boundary values of the PGA identifying the three regions discussed above slightly differ for each case. Interestingly, the layout with a single panel ($N = 1$) always returns the lowest value of the objective function for assigned PGA (that is, the highest efficiency). Further, in this case, α_{ex} and α_{in} have approximately the same value (however, in this layout, only one external link is present, therefore α_{ex} plays a minor role).

5. Removing external or internal links

Based on the trend observed in the previous section, two further optimisation campaigns have been performed removing, in turns,

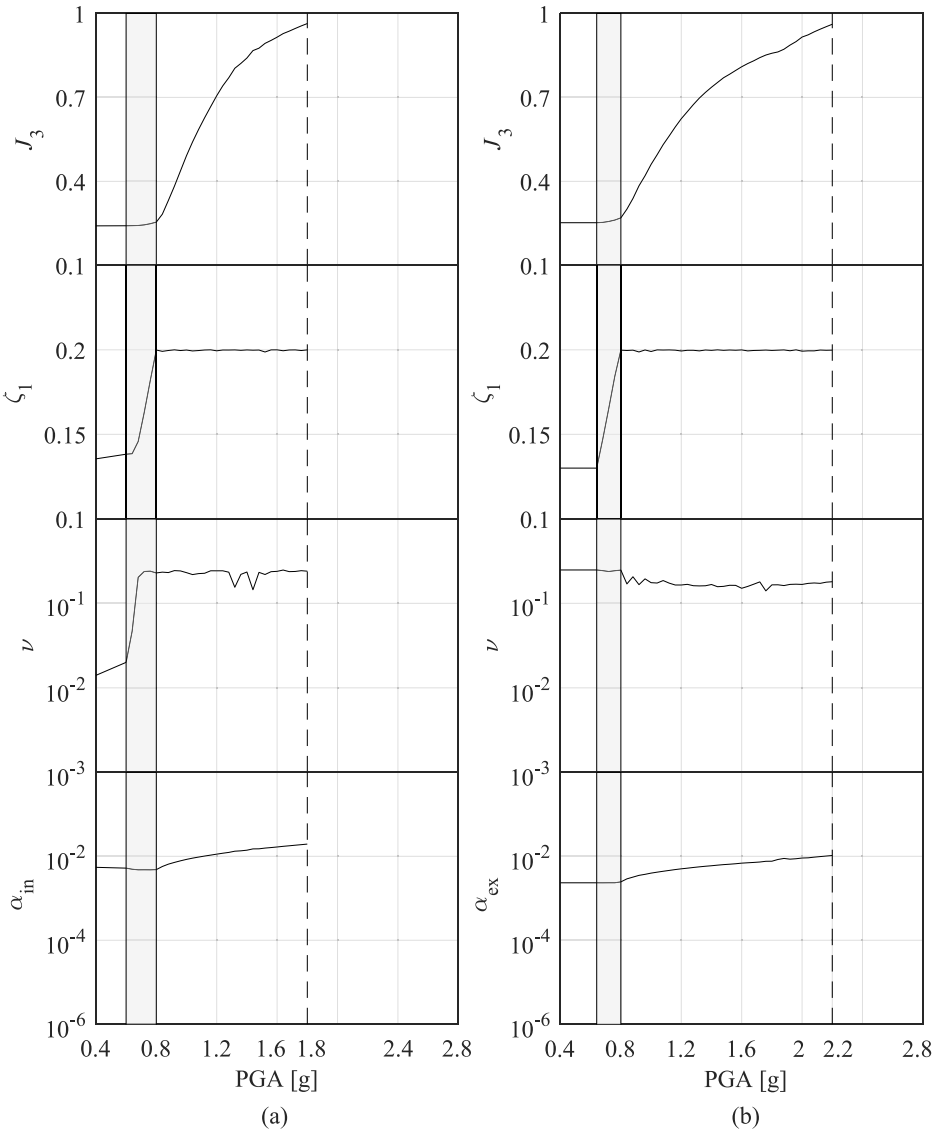

Fig. 7. Objective functions and optimal design parameters for 3-panels layouts considering: (a) $\alpha_{ex} = 0$ and (b) $\alpha_{in} = 0$.

external and internal links between primary frame and DSF panels (corresponding to the cases where either $\alpha_{ex} = 0$ or $\alpha_{in} = 0$, respectively).

The results for the layout with $N = 3$ panels are summarised in Fig. 7. In particular:

- When $\alpha_{ex} = 0$, the maximum value of the PGA for which the constraint cannot be satisfied is $a_g = 1.8\,g$ (reduced by 36% with respect to the four-parameter optimisation). The dynamic behaviour of the optimal DSFs resembles the one discussed above, and in particular three main regions with very similar characteristics can be identified. In the first region (Fig. 7(a)), however, a relatively small increase of both damping ratio and flexural stiffness of the DSF panels is required to keep the same level of efficiency (as measured by the objective function J). The second and third regions instead follow the same trends described for the four-parameter case, with a sharp increase of ζ_1 and ν first, followed by a gradual decrease in efficiency.
- When $\alpha_{in} = 0$, the DSF shows an intermediate performance (Fig. 7(b)) in comparison to the previous two cases, as demonstrated by the intermediate value of the maximum PGA ($a_g = 2.2\,g$) for which the nonlinear constraint can be satisfied. Also in this case, three regions with very similar characteristics can be identified. Interestingly, for this configuration only the damping ratio ζ_1 increases in the second region to keep roughly a constant level of efficiency, while satisfying the nonlinear constraint.

Similar results are observed for the remaining two DSF layouts

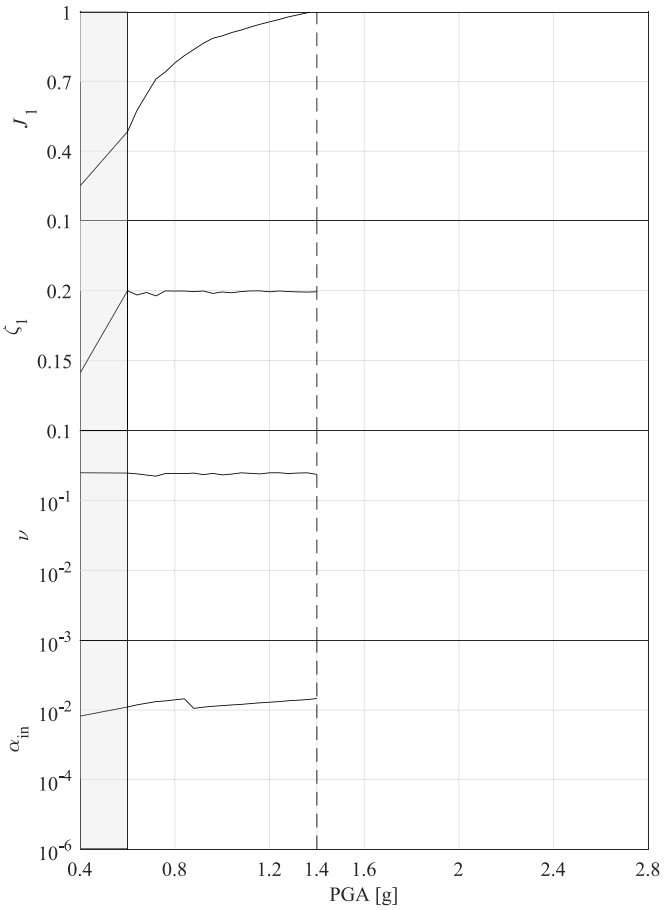

Fig. 8. Objective function and optimal design parameters for 1-panel layout.

(Figs. 8 and 9). For the layout with a single panel ($N = 1$), due to presence of only one α_{ex}-type link at the top of the building, the condition $\alpha_{in} = 0$ does not return any valid solution, while optimal solutions can be found for the case $\alpha_{ex} = 0$ up to a maximum PGA of 1.4 g (see Fig. 8). Comparatively, the layout with two panels ($N = 2$), spanning three storeys each, shows a better performance, as the maximum PGA for which optimal solutions can be found are $a_g = 1.6$ g for the case α_{ex} (i.e. DSF panels with cantilevered ends) and $a_g = 2.4$ g for the case $\alpha_{in} = 0$ (i.e. simply-supported DSF panels), showing the same trends as the one observed for the layout with three panels (see Fig. 9(a) and (b), respectively).

6. Using the same type of link for all connections

In a realistic scenario, using a single type of elastic springs for all the connections could constitute a technical advantage in the construction phase. Moreover, reducing the number of design variables entails lower computational effort. Hence, in this section, the result of the optimisation problem are presented under the assumption that $\alpha_{ex} = \alpha_{in} = \alpha$, therefore reducing the problem to three design variables. As a consequence, a 20% reduction in computational time has been observed in our analyses, performed using a Intel Core i5-5200 CPU @2.2 GHz equipped with 8 GB of RAM. For each PGA value, while the problem involving 4 design variables entailed a computational effort of 2.8 h, only 2.5 h were required for the case of 3 design variables. Results are presented herein for the layout with three DSF panels ($N = 3$), and compared with those shown in Section 4 for the case of four design variables (Fig. 10).

The first notable thing is that the efficiency of the new configuration with a single type of link is comparable with the previous one. In fact, the maximum difference between the two design cases is less than 2%, meaning that, although different solutions are found by the optimisation algorithm, the actual efficiency gain achieved by specifying two different values of link stiffness is negligible from an engineering perspective. Analogously, the difference in the optimal viscous damping ratio ζ_1 is practically negligible for any value of PGA. More in detail, it is possible to identify the same three regions as in the four-parameter optimisation, with increasing ζ_1 in the second region, and constant values of ζ_1 in the first and last regions. With regards to the panel stiffness, while optimising four parameters returned increasing optimal values of ν for increasing PGA, here the trend is inverted. Finally, the optimal link stiffness α shows intermediate values between α_{ex} and α_{in} determined in Section 4, maintaining a constant value in the first region and monotonically increasing in the second and third regions.

Fig. 11 shows the first modal shapes of the DSF panels normalised with respect to the maximum modal displacement, as obtained for the 4-parameters and 3-parameters optimisations (i.e. external and internal links with different stiffness in the first case, and equal stiffness in the second one). In the first case, it has been observed that the modal shapes of the panels, considered as systems independent of the primary building, show two possible qualitative behaviours, depending on the value of the PGA (Fig. 11(a) for PGA ≤ 0.96 g, and Fig. 11(b) in the other cases). In fact, for the top panel in particular:

- when PGA ≤ 0.96 g, the optimal design solution entails $\alpha_{in} > \alpha_{ex}$, hence the central mass act as a pivot point for a quasi-rigid rotation of the top panel.
- when PGA > 0.96 g, the optimal design solution entails $\alpha_{in} < \alpha_{ex}$; as a results all masses in the panel oscillate in phase with each other, with the central mass showing the largest displacements.

For the 3-parameters optimisation, the modal shapes of the façade panel are independent on the PGA value. In fact, since all the links have the same stiffness by design, all the masses translate in phases with, approximately, the same magnitude of the displacements (Fig. 11(c)).

6.1. Comparison among DSF layouts

Results of the optimisation for all DSF layouts with a single link type are illustrated in Fig. 12 for increasing PGA. Among the four cases, the configuration with a single panel ($N = 1$) spanning the whole building's height returns the lowest value of the objective function, and this happens consistently for all the examined values of the PGA, hence showing the best performance. Trends for the optimal damping ratio and link stiffness vs. the PGA are similar to those discussed for the 3-panels layout in the previous section. Interestingly, the optimal panels flexural stiffness, ν, is the only parameter which significantly depend on the chosen layout. While for the case of a single panel the optimal value of ν is an increasing function of the PGA, the opposite happens for all the other layouts. Additionally, the higher the number of panels, the lower is the value to which ν converges when the PGA increases. That

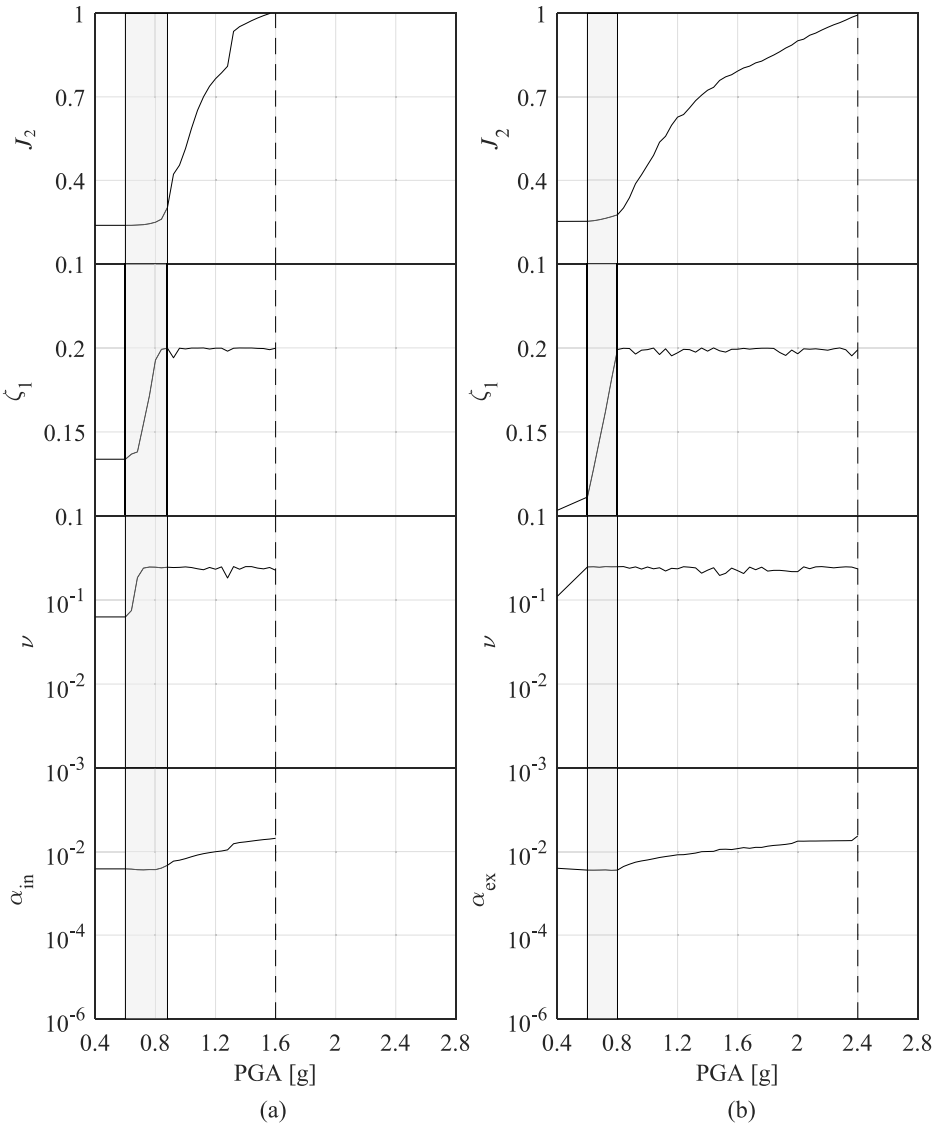

Fig. 9. Objective functions and optimal design parameters for 2-panels layouts considering: (a) $\alpha_{ex} = 0$ and (b) $\alpha_{in} = 0$.

is, the use of fewer and longer panels can provide an efficiency gain, but stiffer panels in flexure are required in the optimal design to exploit this gain.

Fig. 13 shows the absolute value of the transfer function of the uncontrolled structure, in terms of the displacement $x_{0,1}(t)$ of the primary building, say $|H_{0,1}(\omega)|$, i.e. the first element of the vector $|\{\mathbf{H}(\omega)\cdot\mathbf{L}\}|$, compared with the DSF-controlled cases, using each of the four layouts obtained considering the optimal design parameters for (a) $a_g = 0.4\,\mathrm{g}$, (b) $a_g = 0.72\,\mathrm{g}$ and (c) $a_g = 1.6\,\mathrm{g}$. These three design conditions have been chosen in order to highlight any difference in the dynamic behaviour of the primary structure in each of the three regions identified in the previous sections. For ease of comparison, the optimal design parameters for these three values of the IM have been reported in Table 3, showing effectively the same level of performance (i.e. 75% reduction) in the first two regions and the largest allowed viscous damping ratio (i.e. 20%) in the third region. Noticeably, the effect of the optimised DSF panels in the first two regions is similar to what happens in presence of a traditional TMD, as the transfer function shows two distinct peaks replacing the first modal peak for all the four layouts. At higher values of the PGA, on the contrary, the presence of the optimised DSF panels induces: *i*) a shift of the first natural frequency of the combined primary-DSF system towards lower values, beneficial as the corresponding ordinate of the PSD function $G_{\ddot{x}_g}(\omega)$ reduces; *ii*) a reduction in the height of the second and third modal peaks.

6.2. Stochastic versus deterministic frameworks

The proposed stochastic framework assumes the ground motion

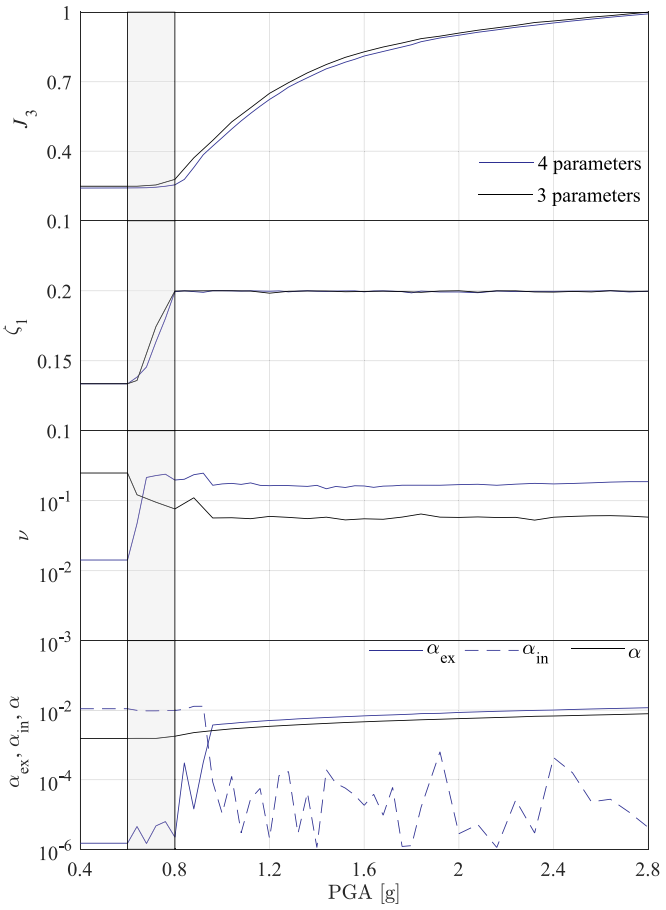

Fig. 10. Objective functions and optimal design parameters for 4 design variables (blue lines) and 3 design variables (black lines), for 3-panels layout.

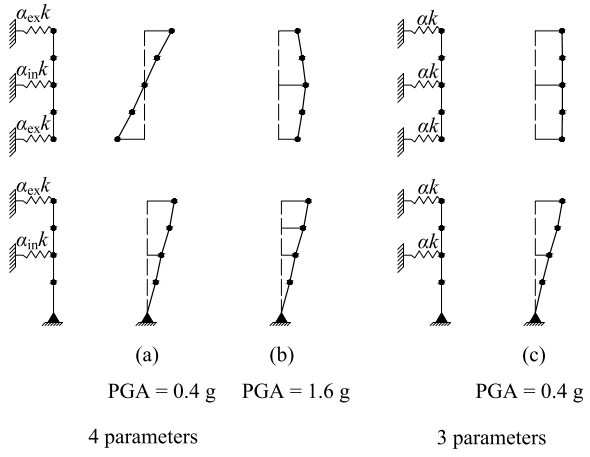

Fig. 11. First modal shapes of the 3-panels layouts using the optimal design variables for: PGA = 0.4 g (a) and (c); PGA = 1.6 g (b).

process $\ddot{x}_g(t)$ as stationary, so to achieve higher computational efficiency. Therefore, a set of further analyses have been carried out, aimed at investigating the effects of this assumption on the optimal design of

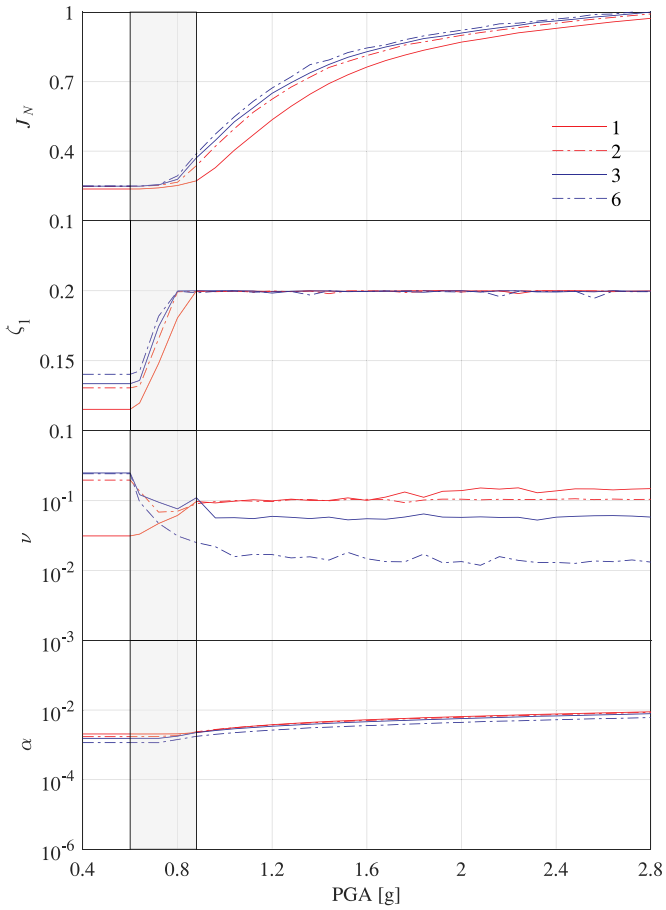

Fig. 12. Objective functions and optimal design parameters for with 3 design variables and different layouts: 1-panel (red solid line), 2-panels (red dashed line), 3-panels (blue solid line) and 6-panels (blue dashed line).

the DSF panel. Specifically, the results of the proposed approach have been compared with the outcomes of the deterministic approach presented in Ref. [25], by utilising the accelerograms reported in Table 1, i.e. the earthquake records used to define the shape of the ED spectrum. In this case, at each step of the optimisation, first the value of the variance of the structural response (normalised with respect to the uncontrolled configuration) is determined for each of the 20 earthquake records, $e = 1, 2, \cdots, 20$; then, the objective function is computed as:

$$\widetilde{J}_N = \frac{1}{20} \sum_{e=1}^{20} \frac{\sigma^2(x_{e,0,1}^{(c)})}{\sigma^2(x_{e,0,1}^{(u)})}. \tag{18}$$

The computation of the function $\widetilde{J}_N$ is done by integrating numerically in the time domain the equations of motion of the coupled dynamic system, for each set of design parameters required by the optimisation algorithm, and for each deterministic earthquake record.

The results of the stochastic and deterministic optimisations are compared in Fig. 14 for the DSF layout with $N = 3$ panels, confirming the robustness of the proposed procedure. In fact, despite its underpinning stationary assumption, the stochastic approach returns roughly the same values of optimal design variables ζ_1, ν, α obtained by using the deterministic optimisation, which accounts fully for the non-

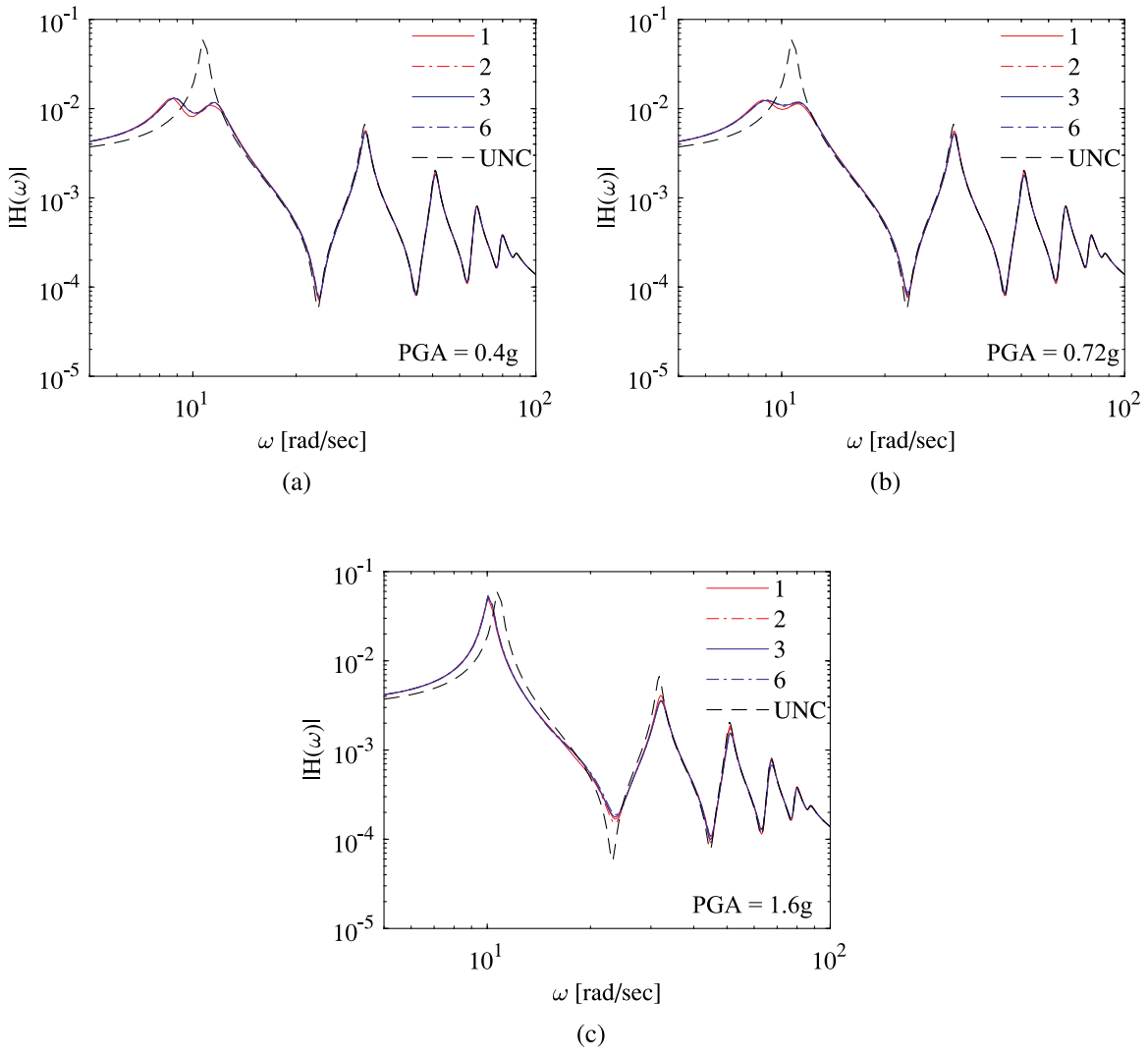

Fig. 13. $H(\omega)$ for DSF layouts 1, 2, 3 and 6 -panels versus also uncontrolled case (black dashed line), using the optimal parameters obtained for load conditions (a) PGA = 0.4g, (b) PGA = 0.72g and (c) PGA = 1.6g.

Table 3
Optimal design parameters for different values of PGA and the four different DSF layouts.

PGA [g]	N	J_N	ζ_1	ν [$\times 10^{-2}$]	α [$\times 10^{-3}$]
0.40	1	0.24	0.12	3.13	2.05
	2	0.25	0.13	19.6	1.72
	3	0.25	0.13	24.8	1.53
	6	0.25	0.14	24.2	1.16
0.72	1	0.24	0.15	4.70	2.05
	2	0.25	0.17	6.85	1.74
	3	0.25	0.17	9.50	1.54
	6	0.26	0.18	4.75	1.15
1.60	1	0.76	0.20	10.1	5.27
	2	0.81	0.20	10.4	5.02
	3	0.83	0.20	5.50	4.62
	6	0.85	0.20	1.48	3.58

stationarity of the seismic input. Importantly, this excellent agreement can be seen for all the three regions of “low”, “medium” and “high” seismicity, i.e. independently of the value of the PGA. The main difference is that the stochastic approach tends to overestimate the performance of the DSF, up to 25% (i.e. the optimised objective function J_3 shows consistently lower values than $\widetilde{J}_3$). On the other hand, since the stochastic approach operates directly in the frequency domain, it allows a massive reduction in terms of computational effort, which can be quantified as about 80% with respect to the deterministic optimisation for the case-study structure (specifically, for each optimisation, 12 hours were needed for the deterministic approach versus 2.5 hours for the stochastic one). Similar agreement has been observed for the other DSF configurations, whose results have not been reported herein to limit the overall number of plots in the manuscript.

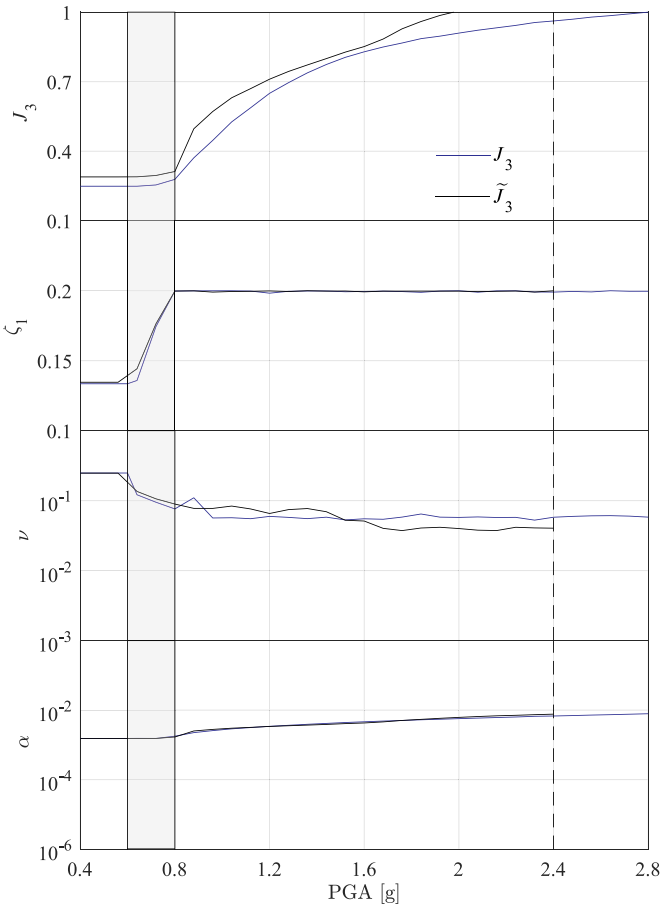

Fig. 14. Objective functions and optimal design parameters for the stochastic case J_3 (blue lines) and the deterministic one $\widetilde{J}_3$ (black lines).

7. Conclusions

A novel stochastic approach to the optimal design of DSFs for passive control of seismic induced vibrations has been presented. Within a 2D setting, four layouts have been analysed, each entailing a different number of independent panels, connected to the main structure through elastic links. The design of the DSF has been approached as an optimisation problem, minimising the inter-storey drifts of the main structure constrained with respect to the maximum relative displacements between the DSF and the building. In first instance, four optimal design parameters have been found, which are the panel damping ratio, stiffness of the DSF panel and of the connection elements, the latter assumed of two types. The seismic excitation has been modelled as a stationary stochastic process with assigned analytic PSD function, consistent with a target ED spectrum. The analyses have been carried out considering increasing values of the PGA, up to 2.8g. In fact, for larger values, no optimal solution able to satisfy the assigned constraints has been found. Three regions have been identified, characterised by different patterns of the optimal design parameters and system dynamic behaviour:

1. In the lowest range of PGA values, the nonlinear constraint plays no role in the optimisation of the DSF. Inside this region all the design variables maintain constant optimal values with no changes in the efficiency of the control system.
2. For intermediate PGA values, the panels' damping ratio and flexural stiffness play a major role on controlling the constraint violation. In particular, in this region the panel's damping ratio increases to its upper boundary value with small variations of PGA. Conversely, the loss of efficiency of the DSF is very small.
3. In the highest range of PGAs, both the panel damping ratio and flexural stiffness have roughly constant values, and the relative displacements of the primary and secondary structures are only controlled by the link elements. Therefore, optimal solutions entail stiffer links and large losses of efficiency of the control system.

An analysis of the performance of the DSF when removing, alternately, external and internal elastic links has been carried on. While results remain qualitatively similar, the lack of connection leads to constraint violation for lower PGA values. In fact, the operative range of the DSF is smaller than the one obtained considering all the links, which proves the importance to ensure a connection at every storey level between DSF and building. As alternative, a design approach using a single type of links between façade and primary structure has been analysed, which constitutes also a practical advantage. The results are in agreement with those obtained considering two types of links. In particular: *i*) the maximum PGA value is approximately the same, while the efficiency is only slightly worse (about 2% difference); *ii*) the panel damping ratio and the link stiffness values show similar trends. The only notable difference is the variation of the panel flexural stiffness against PGAs. In fact, in the lower PGA range, configurations with multiple panels are characterised by stiffer panels with respect to the single panel layout. The inverse is also true in the highest range of PGAs. Additionally, the use of only 3 design variables allow for considerable savings in computational time when performing the optimisation. A comparison among the 4 DSF layouts is discussed, showing how the design with one single panel is the most efficient in the PGA range considered. It has been also observed that, while in the first two PGA intervals the primary effect of the DSF is to significantly dampen the first mode of the main structure, for higher PGAs the DSF mainly causes a shift of the first modal frequency, and a reduction of second and third modal peaks.

Finally, the stochastic optimisation presented in this paper has been compared with a deterministic approach performed using non-stationary earthquake records. The optimal design variables obtained with both procedures have shown excellent agreement. The stochastic framework tends to overestimate the performance of the DSF, but granting a significant saving in computational time (roughly 80%).

Further research on the efficiency and optimal design of DSFs for passive control of wind-excited vibration and analysis of multi-hazard scenarios is currently under development. Future analyses will also look at the use of 3D FE (finite element) models to quantify the effectiveness of the proposed strategy for building structures with irregularities in plan and in elevation.

Declaration of Competing Interest

None.

Appendix A. Seismic PSD closed-form expressions

In the following, for the sake of completeness, the closed-form expressions proposed by Barone et al. [2,3] to compute the parameters of the PSD function starting from those of the ED spectrum are reported:

$$e_1 = 3 - L(\omega_D); \tag{A.1a}$$

$$e_2 = 1 - L(\omega_C); \tag{A.1b}$$

$$e_3 = -1 - \gamma - \beta_2 L(\omega_C); \tag{A.1c}$$

$$e_4 = -1 - \gamma - \beta_3 \left(L(\omega_B) + 2\frac{a_g - 1}{a_g} \right); \tag{A.1d}$$

$$G_0 = \frac{\gamma^2}{\beta_2 \omega_C} \left(\frac{a_g S_0}{\eta_U(\omega_C)} \right)^2, \tag{A.1e}$$

where:

$$\gamma = \frac{4\zeta}{\pi - 4\zeta}; \tag{A.2a}$$

$$L(\omega) = 2\omega \frac{d}{d\omega} \log(\eta_U(\omega)); \tag{A.2b}$$

$$\beta_2 = \left(\frac{\omega_D}{\omega_C} \right)^{e_2+1} \frac{\gamma + e_1 + 1}{e_1 + 1} + \left(1 - \left(\frac{\omega_D}{\omega_C} \right)^{e_2+1} \right) \frac{\gamma + e_2 + 1}{e_2 + 1}; \tag{A.2c}$$

$$\beta_3 = \left(\frac{\omega_C}{\omega_B} \right)^{e_3+1} \beta_2 + \left(1 - \left(\frac{\omega_C}{\omega_B} \right)^{e_3+1} \right) \frac{\gamma + e_3 + 1}{e_3 + 1}, \tag{A.2d}$$

with $\zeta = 0.05$.

References

[1] Ali MM, Moon KS. Structural developments in tall buildings: current trends and future prospects. Archit Sci Rev 2007;50(3):205–23.

[2] Barone G, Lo Iacono F, Navarra G, Palmeri A. A novel analytic model of power spectral density function coherent with earthquake response spectra. 1st International conference on uncertainty quantification in computational sciences and engineering, UNCECOMP 2015, Crete, Greece. 2015. p. 394–406. https://doi.org/10.7712/120215.4280.805.

[3] Barone G, Lo Iacono F, Navarra G, Palmeri A. Closed-form stochastic response of linear building structures to spectrum-consistent seismic excitations. Soil Dyn Earthquake Eng 2019;125. https://doi.org/10.1016/j.soildyn.2019.105724. 105724, 13 pages

[4] Bedon C, Amadio C. Enhancement of the seismic performance of multi-storey buildings by means of dissipative glazing curtain walls. Eng Struct 2017;152:320–34. https://doi.org/10.1016/j.engstruct.2017.09.028.

[5] Bedon C, Amadio C. Numerical assessment of vibration control systems for multi-hazard design and mitigation of glass curtain walls. J Build Eng 2018;15:1–13. https://doi.org/10.1016/j.jobe.2017.11.004.

[6] Boake TM, Harrison K, Collins D, Chatham A, Lee R. Understanding the general principles of the double skin façade system. 9th Canadian conference on building science and technology: design and construction of durable building envelopes, Vancouver, BC, Canada. 2003. p. 329–48.

[7] CEN. Eurocode 8: design of structures for earthquake resistance, Part 1: general rules, seismic actions and rules for buildings, EN 1998-1. Brussels: Comité Européen de Normalisation; 2004.

[8] Chopra AK. Dynamics of structures: theory and applications to earthquake engineering, 4th ed. Pearson Global Edition; 2015.

[9] Constantinou M, Tadjbakhsh I. Optimum design of a first story damping system. Comput Struct 1983;17(2):305–10.

[10] Deb K. An efficient constraint handling method for genetic algorithms. Comput Methods Appl Mech Eng 2000;186(2–4):311–38.

[11] Fu TS. Double skin façades as mass dampers. 2013 American control conference. Washington, DC, USA: IEEE; 2013. p. 4742–6. https://doi.org/10.1109/ACC.2013.6580571.

[12] Gratia E, De Herde A. Natural cooling strategies efficiency in an office building with a double-skin façade. Energy Build 2004;36(11):1139–52.

[13] Høseggen R, Wachenfeldt BJ, Hanssen SO. Building simulation as an assisting tool in decision making. Case study: with or without a double-skin façade? Energy Build 2008;40(5):821–7.

[14] Kareem A, Kline S. Performance of multiple mass dampers under random loading. J Struct Eng 1995;121(2):348–61.

[15] Kasinos S, Palmeri A, Lombardo M. Seismic response of combined primary-secondary structures with the component-mode synthesis method. 15th International conference on civil, structural and environmental engineering computing, CIVIL-COMP 2015, Prague, Czech Republic. 2015. 20 pages

[16] Mahmoud MS, Zribi M, Soh YC. Optimal control of seismically-excited building structures. Comput Struct 2000;74(5):521–33.

[17] Marano GC, Sgobba S, Greco R, Mezzina M. Robust optimum design of tuned mass dampers devices in random vibrations mitigation. J Sound Vib 2008;313(3–5):472–92.

[18] MATLAB. Release 2017b. Natick, Massachusetts: The MathWorks Inc.; 2017.

[19] Mohebbi M, Shakeri K, Ghanbarpour Y, Majzoub H. Designing optimal multiple tuned mass dampers using genetic algorithms (GAs) for mitigating the seismic response of structures. J Vib Control 2013;19:605–25.

[20] Moon KS. Structural design of double skin façades as damping devices for tall buildings. Procedia Eng 2011;14:1351–8.

[21] Morga M, Marano GC, Greco R. Optimization of tuned mass dampers subject to non-stationary random excitation. 15th International conference on civil, structural and environmental engineering computing, CIVIL-COMP 2015, Prague, Czech Republic. 2015. 16 pages

[22] Nigam N. Structural optimization in random vibration environment. AIAA J 1972;10(4):551–3.

[23] Palmeri A, Barone G, Khetawat A. Passive control of building structures using double-skin façades as vibration absorbers. 15th International conference on civil, structural and environmental engineering computing, CIVIL-COMP 2015, Prague, Czech Republic. 2015. 12 pages

[24] Parsaeimaram M, Congqi F, Luo X, Shakya C. Seismic performance evaluation of double skin semi-base-isolated building using incremental dynamic analysis. Adv Civ Eng 2018. https://doi.org/10.1016/j.soildyn.2019.105724. 2747836, 19 pages

[25] Pipitone G, Barone G, Palmeri A. Optimal design of double-skin façades as vibration absorbers. Struct Control Health Monit 2018;25(2). https://doi.org/10.1002/stc.2086. e2086,16 pages

[26] Vamvatsikos D, Cornell C. Developing efficient scalar and vector intensity measures for IDA capacity estimation by incorporating elastic spectral shape information. Earthquake Eng Struct Dyn 2005;34(13):1573–600. https://doi.org/10.1002/eqe.496.

[27] Vanmarcke E. Properties of spectral moments with applications to random vibration. J Eng Mech DivASCE 1972;98(2):425–46.

[28] Villaverde R. Fundamental concepts of earthquake engineering. CRC Press; 2009.